Relaxation dynamics of an exactly solvable electron-phonon model

D. M. Kennes and V. Meden
Institut für Theoretische Physik A and JARA-Fundamentals of Future Information Technology, RWTH Aachen University, 52056 Aachen, Germany

(Received 28 May 2010; revised manuscript received 9 July 2010; published 12 August 2010)

We address the question whether observables of an exactly solvable model of electrons coupled to (optical) phonons relax into large time stationary state values and investigate if the asymptotic expectation values can be computed using a stationary density matrix. Two initial nonequilibrium situations are considered. A sudden quench of the electron-phonon coupling, starting from the noninteracting canonical equilibrium at temperature T in the electron as well as in the phonon subsystems, leads to a rather simple dynamics. A richer time evolution emerges if the initial state is taken as the product of the phonon vacuum and the filled Fermi sea supplemented by a highly excited additional electron. Our model has a natural set of constants of motion, with as many elements as degrees of freedom. In accordance with earlier studies of such type of models, we find that expectation values which become stationary can be described by the density matrix of a generalized Gibbs ensemble which differs from that of a canonical ensemble. For the model at hand, it appears to be evident that the eigenmode occupancy operators should be used in the construction of the stationary density matrix.

DOI: 10.1103/PhysRevB.82.085109 PACS number(s): 71.38.−k, 71.10.Pm, 02.30.Ik, 05.70.Ln

I. INTRODUCTION

It is of fundamental interest to reveal the conditions under which an isolated quantum system for $t\to\infty$ relaxes into a state that can be described by a stationary density matrix. Furthermore, a detailed understanding of the relaxation process is desirable. We here characterize relaxation by considering the time evolution of expectation values of observables. Starting out from a nonequilibrium situation at $t=0$ described by the initial density matrix $\hat{\rho}_\mathrm{i}$ we ask whether the expectation value,

$$\langle \hat{O}_\mathrm{l}\rangle_{\hat{\rho}(t)} = \mathrm{Tr}[\hat{\rho}(t)\hat{O}_\mathrm{l}] \tag{1}$$

of a *local observable* $\hat{O}_\mathrm{l}$ for time $t\to\infty$ approaches a constant value which can also be computed considering the stationary density matrix $\hat{\rho}_\mathrm{st}$,

$$\lim_{t\to\infty}\langle \hat{O}_\mathrm{l}\rangle_{\hat{\rho}(t)} = \mathrm{Tr}[\hat{\rho}_\mathrm{st}\hat{O}_\mathrm{l}]. \tag{2}$$

Here $\hat{\rho}(t)$ denotes the statistical operator at time t which follows from solving the von Neumann equation for the given initial condition $\hat{\rho}(t=0)=\hat{\rho}_\mathrm{i}$. A "local observable" is defined as one which only contains degrees of freedom from a subsystem $\mathcal{S}$ of the isolated quantum system $\mathcal{Q}$. We focus on measurements in subsystems and one must thus be careful in interpreting $\hat{\rho}_\mathrm{st}$ as the density matrix describing the stationary state of the entire quantum system $\mathcal{Q}$. For a meaningful description of the stationary state $\hat{\rho}_\mathrm{st}$ should be independent of the chosen observable. To avoid recurrence effects one has to perform the thermodynamic limit of $\mathcal{Q}$ which is often done by taking the thermodynamic limit $V_\mathcal{E}\to\infty$, with the volume $V_\mathcal{E}$ of the *environment* $\mathcal{E}=\mathcal{Q}/\mathcal{S}$, keeping $V_\mathcal{S}$ fixed.

Relaxation to a time-independent expectation value in the strict sense can only occur after the thermodynamic limit has been taken. Alternatively one can address the question whether a "quasistationary state" is reached in a *finite* system. By this we understand a situation in which expectation values "fluctuate" around a constant value which can be extracted by averaging over time. If such a state is reached one can ask if the time-averaged value can be computed using a stationary statistical ensemble. In the averaging, it might even be meaningful to increase the time interval beyond the characteristic time $t_\mathrm{r}=L/v$—denoted recurrence time in what follows—with L being a typical length and v a typical velocity of the system (see below).

In *equilibrium* statistical physics, we commonly work with *thermal* ensembles as the ones describing the state. They are characterized by the density matrix,

$$\hat{\rho} = \frac{1}{Z}e^{-\sum_{j=1}^{n}\eta_j\hat{I}_j}, \quad Z = \mathrm{Tr}\; e^{-\sum_{j=1}^{n}\eta_j\hat{I}_j} \tag{3}$$

with the partition function $Z(\{\eta_j\})$. The sum usually runs over only a few terms containing operators $\hat{I}_j$, such as the Hamiltonian $\hat{H}$ and the particle number operator $\hat{N}$ corresponding to the macroscopic variables energy and particle number. The Lagrange multipliers η_j are fixed such that the expectation values of the $\hat{I}_j$ take given values $I_j^{(0)}$ (e.g., given average energy and particle number),

$$\langle \hat{I}_j\rangle_{\hat{\rho}} = I_j^{(0)}.$$

Choosing the corresponding Lagrange parameters in Eq. (3) maximizes the entropy $S=\mathrm{Tr}[\hat{\rho}\ln\hat{\rho}^{-1}]$ under the constraint of fixed $I_j^{(0)}$.[1] Within the observables of a closed system (with fixed particle number), the Hamiltonian plays a special role as in many situations the expectation value of the energy is the only conserved quantity. The corresponding Lagrange multiplier is the inverse temperature $\beta=1/T$ and the thermal ensemble with only the energy expectation value fixed is the *canonical* one.

Jaynes[1] studied generalized ensembles—now commonly referred to as generalized Gibbs ensembles (GGEs)—in which additional observables $\hat{I}_j$ besides the energy are as-

sumed to take a given expectation value (fixed $I_j^{(0)}$) and together with the corresponding Lagrange multipliers enter the sum in Eq. (3).

Starting out with the initial nonequilibrium state given by $\hat{\rho}_\mathrm{i}$ and under the assumption that $\langle \hat{O}_\mathrm{l} \rangle_{\hat{\rho}(t)}$ converges for $t \to \infty$ one might expect that the stationary expectation value can be computed from Eq. (2) with $\hat{\rho}_\mathrm{st} = \hat{\rho}_\mathrm{can}$ and

$$\hat{\rho}_\mathrm{can} = e^{-\beta \hat{H}} / Z_\mathrm{can}. \tag{4}$$

This is known as *thermalization*. The inverse temperature β is set by the constraint,

$$\langle \hat{H} \rangle_{\hat{\rho}_\mathrm{can}} = \langle \hat{H} \rangle_{\hat{\rho}_\mathrm{i}}.$$

In particular, this is the expected behavior if the energy is the *only* (independent) constant of motion.

Recent experiments in the field of ultracold atoms[2] led to a revived interest into relaxation dynamics. Due to the long coherence time such systems are ideal candidates to study the relaxation into a stationary state in a controlled setup. In the experiments, an equilibrium state is disturbed by a sudden *quench* of system parameters. The experiments led to several interesting theoretical studies in which models, usually considered in the field of quantum many-particle physics, were investigated concerning their relaxation properties. In analogy to the experiments in most theoretical studies, the system is assumed to be in an *eigenstate* (e.g., the noninteracting ground state) or a *canonical thermal state* with fixed temperature T of the *initial* many-body Hamiltonian $\hat{H}_\mathrm{i}$. At $t=0$ model parameters, in most cases the two-particle interaction being a crucial element of the models, is quenched instantaneously to a different value and the dynamics of the initial state under the time evolution given by the final Hamiltonian $\hat{H}_\mathrm{f}$ is computed.

The investigations can be grouped in three classes. Analytical studies of models which can be solved exactly,[3–11] numerical studies,[12–17] and approximate analytical studies.[18,19] For most of the considered models, the relaxation properties of a restricted set of observables was computed. A more general perspective on the problem for a certain class of models is taken in Refs. 20 and 21 using methods of boundary critical phenomena and conformal field theory. The ultimate goal of the "case studies" is (i) to derive criteria which *a priori* allow to answer the question whether certain (local) observables become stationary and (ii) to construct the stationary density matrix $\hat{\rho}_\mathrm{st}$, corresponding to the appropriate ensemble by which the asymptotic expectation values can be computed. It is of particular interest to understand the conditions under which the latter becomes the canonical one and the system thermalizes. From our considerations, it is plausible to expect that the number and character of the constants of motion of a specific model are of crucial importance in answering the questions addressed above. Roughly speaking, if the number of constants of motion is large, the time-evolved state contains a lot of information from the initial state and thermalization cannot be expected. In all the studies mentioned above single-component systems containing either bosons or fermions were studied. Besides the asymptotic long-time behavior transient nonequilibrium effects such as "collapse and revival" were investigated.

From the analytical[4,5,7,9–11,20] and numerical[13,17] studies of exactly solvable models increasing evidence was collected that *if* the expectation value of an observable $\hat{O}$ approaches a constant large time limit, the latter cannot be obtained using the thermal canonical density matrix. Instead stationary density matrices of the GGE type Eq. (3), corresponding to situations with more restrictions (than a fixed average energy) set by the initial state having a density matrix,

$$\hat{\rho}_\mathrm{GGE} = \frac{1}{Z_\mathrm{GGE}} e^{-\sum_{j=1}^{n} \eta_j \hat{I}_j}, \quad Z_\mathrm{GGE} = \mathrm{Tr}\, e^{-\sum_{j=1}^{n} \eta_j \hat{I}_j} \tag{5}$$

turned out to be promising candidates. On the basis of the above considerations this is not surprising, as the models considered are characterized by more integrals of motion than just the energy and one thus expects for the stationary state an increased "memory" of the initial state. A set of constants of motion were taken as the $\hat{I}_j$ and the Lagrange multipliers η_j were determined such that

$$\langle \hat{I}_j \rangle_{\hat{\rho}_\mathrm{i}} = \langle \hat{I}_j \rangle_{\hat{\rho}_\mathrm{GGE}}. \tag{6}$$

The choice of conserved observables is not unique. For example, with $\hat{H}$ being a constant of motion the same holds for $\hat{H}^2$, and it was shown[11] that under certain conditions the GGE expectation value of a given observable $\hat{O}$,

$$\langle \hat{O} \rangle_{\hat{\rho}_\mathrm{GGE}} = \mathrm{Tr}[\hat{\rho}_\mathrm{GGE} \hat{O}] \tag{7}$$

might depend on the selected set. Thus the GGE describes the stationary state only if the "correct" set of "independent" $\hat{I}_j$ is chosen. For a general model with several possible sets of constants of motion up to now it is not clear how to select the correct set *a priori*.

In cases in which the system's Hamiltonian can be brought into the form

$$\hat{H} = \sum_k \lambda(k) \hat{\psi}_k^\dagger \hat{\psi}_k \tag{8}$$

with either fermionic or bosonic creation and annihilation operators $\hat{\psi}_k^{(\dagger)}$ and quantum number k the eigenmode occupation operators $\hat{n}_k = \hat{\psi}_k^\dagger \hat{\psi}_k$ constitute a natural set of conserved quantities, with as many elements as degrees of freedom. Then the statistical expectation value taken with the ρ_GGE set up with $\hat{I}_k = \hat{n}_k$ and Lagrange multipliers fixed by the constraints Eq. (6) led for generic model parameters to the correct large time limit of (certain) observables *provided* the latter exists[5,9,11] and the initial states are homogeneous.[22]

Cold-atom gases is not the only subfield of modern condensed-matter physics in which understanding the relaxation dynamics is of crucial importance and quenches are not the only process leading to an interesting time evolution. In the area of photoexcited semiconductors, much effort has been put into measuring (pump-probe techniques) and understanding the relaxation dynamics of highly excited electrons coupled to optical phonons; for a recent review see Ref. 23. The long-time asymptotics of the electron-phonon system is

difficult to study experimentally due to the strong coupling to other degrees of freedom (e.g., acoustic phonons and holes) but the short-time (transient) dynamics shows interesting non-Markovian effects requiring a treatment beyond the use of Boltzmann equations.[23–26] A detailed understanding of relaxation also plays a major role in the field of condensed-matter system based quantum information processing.[27] Here the strong coupling of the degrees of freedom envisaged as quantum bits to the environment usually leads to a coherence time to short to perform substantial information processing. Gaining insights into the relaxation process might lead to ways to circumvent this obstacle and significantly increase the coherence time.

We here supplement the recent case studies on the relaxation dynamics of either bosonic or fermionic correlated systems by analytically investigating the time evolution of a *two-component* model of electrons coupled to phonons. The model naturally contains two subsystems—the electron and the phonon systems—and an observable can be considered as *local* if it contains only fermionic or bosonic degrees of freedom. We first consider the time evolution resulting from a quench of the electron-phonon coupling from zero to a finite value starting with the noninteracting canonical equilibrium at temperature T in the electron as well as the phonon subsystems. In *addition* we study the dynamics inferred by the interacting Hamiltonian out of a pure state given by the product of the phonon vacuum and the filled Fermi sea supplemented by a highly excited additional electron of momentum k_0. The *short-time* dynamics of our model starting with this initial state was earlier discussed in the context of optically excited semiconductors[25] and used to explain results of pump-probe experiments.[24,26] While the time evolution of observables, in particular, the electron or phonon momentum distribution function and the subsystem energies, is rather simple for the quench a rich dynamics is found in case of the "k_0 excitation." We show that in the large time limit $t\to\infty$, the subsystem energies (and the energy in the electron-phonon coupling) converge to stationary values for both nonequilibrium initial states. The same holds for the electron momentum distribution while for the phonon momentum distribution function convergence is only achieved after averaging over a small momentum interval. Our model can be brought into the form Eq. (8). It thus contains (at least) as many constants of motion as degrees of freedom. In accordance with earlier studies,[5,9,11] we find that for both initial states the expectation values of observables which become stationary can be described by the density matrix of a generalized Gibbs ensemble with the eigenmode occupation operators chosen as the $\hat{I}_j$.

The rest of this paper is organized as follows. In Sec. II, we introduce our one-dimensional (1D) electron-phonon model and specify our initial states. The bosonization of the fermionic field operator, which allows to obtain analytical results for the time evolution of fermionic observables, is discussed in Sec. III. Section IV is devoted to the GGE for the model at hand. In Secs. V and VI, we discuss the relaxation dynamics for our two distinct initial states and compare the long-time expectation values to those obtained from the GGE. Finally, our results are summarized in Sec. VII.

II. ELECTRON-PHONON MODEL AND THE NONEQUILIBRIUM INITIAL STATES

We consider a model of electrons on a 1D ring of length L (periodic boundary conditions) coupled to phonons by a Holstein-type electron-phonon interaction given by the Hamiltonian,

$$\hat{H} = \hat{H}_{\mathrm{e}} + \hat{H}_{\mathrm{p}} + \hat{H}_{\mathrm{ep}} \tag{9}$$

with

$$\hat{H}_{\mathrm{e}} = \sum_k \epsilon_k (\hat{a}_k^\dagger \hat{a}_k - \langle \hat{a}_k^\dagger \hat{a}_k \rangle_0), \tag{10}$$

$$\hat{H}_{\mathrm{p}} = \sum_{q>0} \omega_q \hat{B}_q^\dagger \hat{B}_q, \tag{11}$$

$$\hat{H}_{\mathrm{ep}} = \left(\frac{2\pi}{L}\right)^{1/2} \sum_{\substack{k \\ q>0}} g(q)(\hat{a}_{k+q}^\dagger \hat{a}_k \hat{B}_q + \mathrm{H.c.}). \tag{12}$$

Here $\hat{a}_k(\hat{B}_q)$ is the annihilation operator of an electron (phonon) with momentum $k(q)$ and $\langle\cdots\rangle_0$ is the expectation value in the noninteracting ground state (normal ordering). The momentum-dependent electron-phonon coupling is denoted by $g(q)$. To be specific, we consider the (simple) form $g(q)=g\Theta(q_{\mathrm{c}}-q)$. We restrict our considerations to a single branch of chiral (right-moving) spinless fermions with linear single-particle dispersion $\epsilon_k=v_{\mathrm{F}}(k-k_{\mathrm{F}})$, the Fermi velocity v_{F}, and the Fermi momentum k_{F} which, without loss of generality, is set to zero in the following ($k_{\mathrm{F}}=0$). We assume that the fermion states do not have a lower bound (Dirac model) and all momentum states with $k<0$ are filled in the ground state (filled Fermi sea). For the sake of convenience, the Fermi momentum k_{F} corresponds to the first empty instead of the last occupied state. Divergencies possibly resulting from these states are regularized by the normal ordering. Furthermore, we focus on optical phonons (Einstein model) with a single energy $\omega_q=\omega_0$.

The assumed q dependences of the phonon dispersion and the electron-phonon coupling can be relaxed without spoiling the possibility of an exact analytical solution of the model. Varying the function $g(q)$ only leads to minor changes in the short-time dynamics[25] [as long as $g(0)$ remains finite] and we do not see any physical reason why our main results for the *long-time* relaxation obtained here should be dependent on the precise form of $g(q)$. Our model is a variant of the purely fermionic Tomonaga-Luttinger model[28,29]—more precisely what is called the chiral g_4 model[30]—and similar to this case the linear fermion dispersion is crucial for an exact analytic solution. Equilibrium properties of the above model, also considering acoustic instead of optical phonons, were discussed earlier.[31–35] The quench dynamics of the Tomonaga-Luttinger model was studied in Ref. 5.

To diagonalize our Hamiltonian Eqs. (9)–(12), we first introduce the electron density operator,

$$\hat{d}_q = \sum_k \hat{a}_k^\dagger \hat{a}_{k+q} \tag{13}$$

with $q>0$. For $q=0$, we define the electron number operator relative to the ground state (filled Fermi sea) as

$$\hat{N} = \sum_k (\hat{a}_k^\dagger \hat{a}_k - \langle \hat{a}_k^\dagger \hat{a}_k \rangle_0). \tag{14}$$

With a proper normalization, the densities $\hat{d}_q$ obey Bose commutation relations.[29] If one defines

$$\hat{b}_q = \left(\frac{2\pi}{qL}\right)^{1/2} \hat{d}_q, \quad \hat{b}_q^\dagger = \left(\frac{2\pi}{qL}\right)^{1/2} \hat{d}_{-q}, \tag{15}$$

for $q>0$, the commutation relations read

$$[\hat{b}_q, \hat{b}_{q'}^\dagger] = \delta_{q,q'}, [\hat{b}_q, \hat{b}_{q'}] = 0. \tag{16}$$

The electron-hole excitations in H_{ep} can straightforwardly be written linearly in the boson operators b_q and $b_q^\dagger$. For 1D systems with a linear dispersion, it is in addition possible to write the kinetic energy of the fermions as[29,36]

$$H_{\mathrm{e}} = \sum_{q>0} \varepsilon_q b_q^\dagger b_q + c(\hat{N}), \tag{17}$$

where $c(\hat{N})$ only contains the fermionic particle number operator. In the following this term can be dropped because we are working in a sector of the Hilbert space with constant particle number. We can now formulate Eqs. (9)–(12) in terms of the bosonic fermion densities and the phonons as

$$\hat{H} = \sum_{q>0} v_{\mathrm{F}} q \hat{b}_q^\dagger \hat{b}_q + \omega_0 \sum_{q>0} \hat{B}_q^\dagger \hat{B}_q + g \sum_{0<q\leq q_{\mathrm{c}}} \sqrt{q}(\hat{b}_q^\dagger \hat{B}_q + \mathrm{H.c.}). \tag{18}$$

From this expression, it becomes evident that the ground state of the model is still the tensor product of the Fermi sea—corresponding to the vacuum of the bosonic fermion density $\hat{b}_q$—and the phonon vacuum. Therefore, all ground-state expectation values, such as, e.g., the fermionic momentum distribution, are given by the noninteracting ones.

Using a canonical transformation, the problem of the coupled bosonic modes Eq. (18) can be brought in the form of Eq. (8).[31] The transformation is given by

$$\hat{b}_q = \hat{\alpha}_q c_q - \hat{\beta}_q s_q,$$

$$\hat{B}_q = \hat{\alpha}_q s_q + \hat{\beta}_q c_q \tag{19}$$

with

$$c_q^2 = \frac{|\lambda_+(q) - \omega_0|}{\lambda_+(q) - \lambda_-(q)}, \quad s_q^2 = \frac{|\lambda_-(q) - \omega_0|}{\lambda_+(q) - \lambda_-(q)} \tag{20}$$

and the mode energies

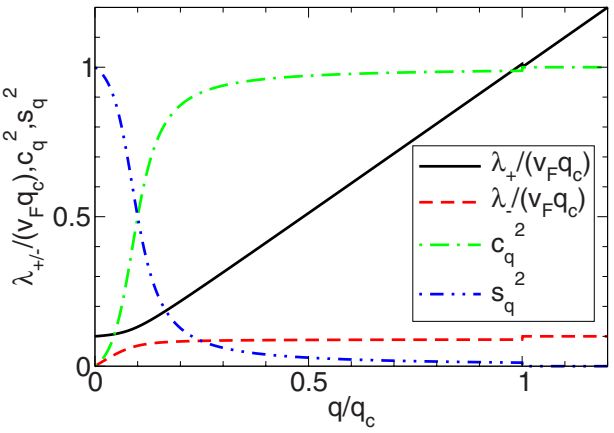

FIG. 1. (Color online) Eigenmodes $\lambda_\pm(q)$ and coefficients c_q^2 and s_q^2 of the eigenvectors for $\Gamma=0.01$ and $\Omega=0.1$. Note the sharp transition (discontinuity) to the noninteracting values at q_c.

$$\lambda_\pm(q) = \frac{1}{2}\{v_{\mathrm{F}} q + \omega_0 \pm \sqrt{(v_{\mathrm{F}} q - \omega_0)^2 + 4g^2 q \Theta(q_{\mathrm{c}} - q)}\}. \tag{21}$$

Note that $c_q^2 + s_q^2 = 1$ for all $q>0$ and that $c_q^2=1$, $s_q^2=0$ for $q>q_{\mathrm{c}}$. Here we focus on the case $v_{\mathrm{F}} q_{\mathrm{c}} > \omega_0$. In the new bosonic operators $\hat{\alpha}_q$ and $\hat{\beta}_q$, the Hamiltonian reads

$$\hat{H} = \sum_{q>0} [\lambda_+(q) \hat{\alpha}_q^\dagger \hat{\alpha}_q + \lambda_-(q) \hat{\beta}_q^\dagger \hat{\beta}_q]. \tag{22}$$

In order to obtain a stable ground state, the boson energies $\lambda_\pm(q)$ have to be larger than zero.[31] For a given ω_0, this leads to a restriction of the coupling strength g that can be used. The dimensionless parameters of the model are $\Gamma = \frac{g^2}{v_{\mathrm{F}} q_{\mathrm{c}}}$ for the electron-phonon coupling, $\Omega = \frac{\omega_0}{v_{\mathrm{F}} q_{\mathrm{c}}}$ for the phonon frequency, and $\nu = \frac{2\pi}{L q_{\mathrm{c}}}$ for the inverse of the ring length. Stability requires that $\Gamma < \Omega$. The momentum dependence of the eigenmode energies $\lambda_\pm(q)$ and the coefficients c_q^2 and s_q^2 are shown in Fig. 1 for a typical set of parameters with $\Gamma=0.01$ and $\Omega=0.1$.

With Eqs. (20) and (22) computing the dynamics of the phonon ladder operators and fermionic densities becomes simple. We find

$$\hat{B}_q(t) = c_q s_q (e^{-i\lambda_+(q)t} - e^{-i\lambda_-(q)t}) \hat{b}_q + (s_q^2 e^{-i\lambda_+(q)t} + c_q^2 e^{-i\lambda_-(q)t}) \hat{B}_q \tag{23}$$

and

$$\hat{b}_q(t) = (c_q^2 e^{-i\lambda_+(q)t} + s_q^2 e^{-i\lambda_-(q)t}) \hat{b}_q + c_q s_q (e^{-i\lambda_+(q)t} - e^{-i\lambda_-(q)t}) \hat{B}_q. \tag{24}$$

The time dependence of expectation values of observables which can be written in terms of the $B_q^{(\dagger)}$ and $b_q^{(\dagger)}$ can thus be expressed by expectation values taken with the initial density matrix $\hat{\rho}_{\mathrm{i}}$. This gives us direct access to the dynamics of the phonon momentum distribution function,

$$N(q,t) = \langle \hat{B}_q^\dagger(t)\hat{B}_q(t)\rangle_{\hat{\rho}_\mathrm{i}} = \langle \hat{B}_q^\dagger(0)\hat{B}_q(0)\rangle_{\hat{\rho}(t)} \tag{25}$$

and that of the subsystem energies for both nonequilibrium states considered. Alternatively with Eqs. (23) and (24) the time evolution of the density matrix can be given in a closed form if $\hat{\rho}_\mathrm{i}$ can be expressed in terms of the $b_q^{(\dagger)}$ and $B_q^{(\dagger)}$ (see below). To compute the fermionic momentum distribution function,

$$n(k,t) = \langle \hat{a}_k^\dagger(t)a_k(t)\rangle_{\hat{\rho}_\mathrm{i}} = \langle \hat{a}_k^\dagger(0)a_k(0)\rangle_{\hat{\rho}(t)}$$

one has to establish a relation between the fermionic operators $a_k^{(\dagger)}$ and the $b_q^{(\dagger)}$. This *bosonization* (of the field operator) will be discussed in Sec. III.

We consider two different initial situations at time $t=0$. In the first one, the *decoupled* ($g=0$) electron-phonon system is initially assumed to be in a thermal state with a common temperature $T=1/\beta$ of the electron and phonon subsystems corresponding to the noninteracting canonical ensemble. It is determined by the initial density matrix (superscript q for "quench")

$$\hat{\rho}_\mathrm{i}^\mathrm{q} = e^{-\hat{\beta}H_\mathrm{e}} \otimes e^{-\hat{\beta}H_\mathrm{p}}/Z. \tag{26}$$

The second initial density matrix is given by a *pure state* (superscript k_0 for "k_0 excitation")

$$\hat{\rho}_\mathrm{i}^{k_0} = |\Psi_\mathrm{i}\rangle\langle\Psi_\mathrm{i}| \tag{27}$$

with

$$|\Psi_\mathrm{i}\rangle = \hat{a}_{k_0}^\dagger|\mathrm{FS}\rangle \otimes |\mathrm{vac}\rangle. \tag{28}$$

Here $|\mathrm{FS}\rangle$ denotes the filled Fermi sea (vacuum with respect to the $\hat{b}_q$) and $|\mathrm{vac}\rangle$ the phonon vacuum. One can think of this state being (approximately) realized in a doped semiconductor (Fermi sea in conduction band) in which an additional "hot" electron with momentum k_0 is optically pumped from the valence band into the conduction band. Both initial conditions correspond to nonequilibrium states if the time evolution is performed with the Hamiltonian Eq. (18) for $g \neq 0$. We note in passing that starting out with the noninteracting ground state ($T=0$) would *not* lead to a time dependence of expectation values after a sudden quench of g as in the present model this state remains the ground state even for $g \neq 0$.

III. BOSONIZATION OF THE FERMIONS

To calculate fermionic expectation values such as the momentum distribution function we use the bosonization of the fermionic field operator,

$$\hat{\psi}^\dagger(x) = \frac{1}{\sqrt{L}}\sum_k e^{-ikx}\hat{a}_k^\dagger. \tag{29}$$

One can prove the operator identity[29]

$$\hat{\psi}^\dagger(x) = \frac{e^{-ix\pi/L}}{\sqrt{L}} e^{-i\hat{\Phi}^\dagger(x)}\hat{U}^\dagger e^{-i\hat{\Phi}(x)} \tag{30}$$

with

$$\hat{\Phi}(x) = \frac{\pi}{L}\hat{N}x - i\sum_{q>0} e^{iqx}\left(\frac{2\pi}{Lq}\right)^{1/2}\hat{b}_q, \tag{31}$$

where $\hat{U}^\dagger$ denotes a unitary fermionic raising operator which commutes with the $\hat{b}_q^{(\dagger)}$ and maps the N-electron ground state to the $(N+1)$-electron ground state. As we are interested in the dynamics for a fixed particle number neither the term proportional to $\hat{N}$ in Eq. (31) nor the fermionic raising operator $\hat{U}^\dagger$ affect the result and both can be dropped in the following. Using Eqs. (30) and (31) and the backtransform

$$\hat{a}_k^\dagger = \frac{1}{\sqrt{L}}\int_{-L/2}^{L/2} e^{ikx}\psi^\dagger(x)dx$$

of Eq. (29) as well as Eq. (24) the time dependence of $a_k^{(\dagger)}$ can be expressed in terms of the $b_q^{(\dagger)}$ and $B_q^{(\dagger)}$. As further deepened below this allows us to give a closed expression for the time evolution of the fermionic momentum distribution $n(k,t)$ as well as its value in the appropriate GGE.

IV. GENERALIZED GIBBS ENSEMBLE

As shown in Sec. II, our coupled electron-phonon Hamiltonian can be brought into the diagonal form Eq. (8) with the bosonic operators $\hat{\alpha}_q^{(\dagger)}$ and $\hat{\beta}_q^{(\dagger)}$ and the corresponding mode energies $\lambda_\pm(q)$. Therefore the eigenmode occupancies $\hat{\alpha}_q^\dagger\hat{\alpha}_q$ and $\hat{\beta}_q^\dagger\hat{\beta}_q$ constitute a set of constants of motion which has as many elements as degrees of freedom in our model. The occupancies thus form a natural set of operators $\hat{I}_j$ which can be used to set up the density matrix of a GGE Eq. (5). We again emphasize that in Ref. 11 an example is given, which shows that an alternative choice of conserved I_j might lead to GGE expectation values of observables which differ from the ones obtained by the natural choice. We show here that for our model all the studied observables which become stationary in the long-time limit approach a value consistent with the GGE set up by the set of occupancies (called natural GGE below).

The GGE is described by the density matrix,

$$\hat{\rho}_\mathrm{GGE} = \frac{1}{Z_\mathrm{GGE}} e^{-\Sigma_q \eta_q \hat{\alpha}_q^\dagger\hat{\alpha}_q - \Sigma_q \xi_q \hat{\beta}_q^\dagger\hat{\beta}_q} \tag{32}$$

with the Lagrange multipliers η_q and ξ_q determined by the initial condition,

$$\langle \hat{\alpha}_q^\dagger\hat{\alpha}_q\rangle_{\hat{\rho}_\mathrm{i}} = \langle \hat{\alpha}_q^\dagger\hat{\alpha}_q\rangle_{\hat{\rho}_\mathrm{GGE}} \tag{33}$$

and similarly for $\hat{\beta}_q$. For a density matrix of the form Eq. (32), the eigenmode occupancies are given by[37]

$$\langle \hat{\alpha}_q^\dagger\hat{\alpha}_q\rangle_{\hat{\rho}_\mathrm{GGE}} = n_\mathrm{B}(\eta_q), \quad \langle \hat{\beta}_q^\dagger\hat{\beta}_q\rangle_{\hat{\rho}_\mathrm{GGE}} = n_\mathrm{B}(\xi_q) \tag{34}$$

with the Bose function,

$$n_\mathrm{B}(x) = [e^x - 1]^{-1}.$$

To fix the Lagrange multipliers, we still have to compute the left-hand side of Eq. (33) for the two initial density ma-

trices Eqs. (26) and (27). For the quench we obtain using (the inversion of) Eq. (19),

$$\langle \hat{\alpha}_q^\dagger \hat{\alpha}_q \rangle_{\hat{\rho}_i^q} = c_q^2 n_B(\beta v_F q) + s_q^2 n_B(\beta \omega_0),$$

$$\langle \hat{\beta}_q^\dagger \hat{\beta}_q \rangle_{\hat{\rho}_i^q} = s_q^2 n_B(\beta v_F q) + c_q^2 n_B(\beta \omega_0), \tag{35}$$

which leads to the set of nonlinear equations for the η_q and ξ_q,

$$n_B(\eta_q) = c_q^2 n_B(\beta v_F q) + s_q^2 n_B(\beta \omega_0),$$

$$n_B(\xi_q) = s_q^2 n_B(\beta v_F q) + c_q^2 n_B(\beta \omega_0). \tag{36}$$

Obviously, the η_q and ξ_q are functions of the inverse temperature β.

For the k_0 excitation, it follows using (the inversion of) Eq. (19) and the "vacuum" properties of the initial pure state that

$$\begin{aligned}
\langle \hat{\alpha}_q^\dagger \hat{\alpha}_q \rangle_{\hat{\rho}_i^{k_0}} &= \mathrm{Tr}[\hat{\rho}_i^{k_0} \hat{\alpha}_q^\dagger \hat{\alpha}_q] \\
&= \langle \mathrm{vac}| \otimes \langle \mathrm{FS}| \hat{a}_{k_0} (c_q \hat{b}_q^\dagger + s_q B_q^\dagger) \\
&\quad \times (c_q \hat{b}_q + s_q B_q) \hat{a}_{k_0}^\dagger |\mathrm{FS}\rangle \otimes |\mathrm{vac}\rangle \\
&= c_q^2 \langle \mathrm{FS}| \hat{a}_{k_0} \hat{b}_q^\dagger \hat{b}_q \hat{a}_{k_0}^\dagger |\mathrm{FS}\rangle \\
&= c_q^2 \langle \mathrm{FS}| \hat{a}_{k_0} \hat{b}_q^\dagger ([\hat{b}_q, \hat{a}_{k_0}^\dagger] + \hat{a}_{k_0}^\dagger \hat{b}_q) |\mathrm{FS}\rangle \\
&= c_q^2 \frac{2\pi}{Lq} \langle \mathrm{FS}| \hat{a}_{k_0-q} \hat{a}_{k_0-q}^\dagger |\mathrm{FS}\rangle \\
&= c_q^2 \frac{2\pi}{Lq} \Theta(k_0 - q)
\end{aligned} \tag{37}$$

with the Θ function defined such that $\Theta(0)=1$. In the step from the fourth to the fifth equation, we have used twice that from Eqs. (13) and (15) it follows that

$$[\hat{b}_q, \hat{a}_{k_0}^\dagger] = \sqrt{\frac{2\pi}{Lq}} \hat{a}_{k_0-q}^\dagger.$$

Similarly we obtain

$$\langle \hat{\beta}_q^\dagger \hat{\beta}_q \rangle_{\hat{\rho}_i^{k_0}} = s_q^2 \frac{2\pi}{Lq} \Theta(k_0 - q), \tag{38}$$

which determines the Lagrange parameters using Eqs. (33) and (34).

A. Expectation values for the quench

We are now in a position to determine the GGE expectation values for the subsystem energies, the phonon momentum distribution $N_{\mathrm{GGE}}(q)$, and the fermion momentum distribution $n_{\mathrm{GGE}}(k)$ first focusing on the quench. With Eqs. (18), (19), and (35) we straightforwardly obtain

$$\begin{aligned}
\langle \hat{H}_e \rangle_{\hat{\rho}_{\mathrm{GGE}}} &= \sum_{q>0} v_F q \{ n_B(\beta v_F q) - 2 c_q^2 s_q^2 \\
&\quad \times [n_B(\beta v_F q) - n_B(\beta \omega_0)] \},
\end{aligned}$$

$$\begin{aligned}
\langle \hat{H}_p \rangle_{\hat{\rho}_{\mathrm{GGE}}} &= \omega_0 \sum_{q>0} \{ n_B(\beta \omega_0) + 2 c_q^2 s_q^2 \\
&\quad \times [n_B(\beta v_F q) - n_B(\beta \omega_0)] \},
\end{aligned}$$

$$\langle \hat{H}_{ep} \rangle_{\hat{\rho}_{\mathrm{GGE}}} = 2g \sum_{q>0} \sqrt{q} c_q s_q (c_q^2 - s_q^2) [n_B(\beta v_F q) - n_B(\beta \omega_0)]. \tag{39}$$

The first terms in the subsystem energies are the expectation values taken with the initial canonical ensemble at $g=0$. Without a high momentum cutoff, the energy in the phonon subsystem obviously diverges. Here we avoid to introduce such a cutoff by considering the excess energies $\delta\langle \hat{H}_p \rangle_{\hat{\rho}_{\mathrm{GGE}}} = \langle \hat{H}_p \rangle_{\hat{\rho}_{\mathrm{GGE}}} - \langle \hat{H}_p \rangle_{\hat{\rho}_i^q}$ and $\delta\langle \hat{H}_e \rangle_{\hat{\rho}_{\mathrm{GGE}}}$ (defined similarly) in the following. Note that the momentum sums containing a factor s_q are cut off at q_c as $s_q=0$ for $q>q_c$. With

$$\sum_{q>0} \ldots \to \frac{L}{2\pi} \int_0^\infty dq \ldots$$

for large L, it becomes apparent that the subsystem excess energies and the energy in the electron-phonon coupling are *extensive* and scale $\sim L$.

For the phonon momentum distribution function, it follows similarly that

$$\begin{aligned}
\delta N_{\mathrm{GGE}}(q) &= N_{\mathrm{GGE}}(q) - n_B(\beta \omega_0) \\
&= 2 c_q^2 s_q^2 [n_B(\beta v_F q) - n_B(\beta \omega_0)].
\end{aligned} \tag{40}$$

It is instructive to compare this result to the canonical (equilibrium) phonon distribution of the *interacting* system (same parameters g and ω_0) at some temperature $\tilde{T}=1/\tilde{\beta}$ characterized by the density matrix Eq. (4). A straightforward calculation using the methods introduced above gives

$$N_{\mathrm{can}}(q) = s_q^2 n_B[\tilde{\beta} \lambda_+(q)] + c_q^2 n_B[\tilde{\beta} \lambda_-(q)].$$

Obviously, the q dependences of this function and Eq. (40) differ and no temperature $\tilde{T}$ can be found leading to coinciding results.

Using the method introduced in Sec. III, the Baker-Hausdorff relation, and the formula[37]

$$\langle e^{\hat{A}} e^{\hat{B}} \rangle = e^{\langle \hat{A}^2 + 2\hat{A}\hat{B} + \hat{B}^2 \rangle / 2}$$

one obtains for the fermionic momentum distribution function in the GGE,

$$n_{\mathrm{GGE}}(k) = \frac{1}{L}\int_{-L/2}^{L/2} dx e^{-ikx} \exp\left\{\sum_{q>0}\frac{2\pi}{Lq}e^{-iq(x-i0)}\right\} \times\exp\left\{-\sum_{q>0}\frac{4\pi}{Lq}[1-\cos(qx)]n_{\mathrm{B}}(\beta v_{\mathrm{F}}q)\right\} \times\exp\left\{\sum_{q>0}\frac{8\pi}{Lq}c_q^2 s_q^2[1-\cos(qx)] \times[n_{\mathrm{B}}(\beta v_{\mathrm{F}}q)-n_{\mathrm{B}}(\beta\omega_0)]\right\}. \quad (41)$$

The third factor, which vanishes for $g=0$, contains the information about the electron-phonon coupling. The first two terms constitute the canonical momentum distribution at temperature $T=1/\beta$ for a *noninteracting* fermionic system with linear dispersion on a ring of size L in equilibrium. This $g=0$ expression was earlier derived in Ref. 38. As discussed there it becomes equal to the (grand canonical) Fermi function $[e^{\beta v_{\mathrm{F}}q}+1]^{-1}$ (only) in the thermodynamic limit $L\to\infty$. Instead of numerically performing the sums and the integral for finite L, Eq. (41) can very efficiently be evaluated using an iterative approach introduced in the Appendix of Ref. 38. Adopting this method to the present situation we obtain for $m\in\mathbb{Z}$, $k_m=2\pi m/L$, $l=0,1,2,\ldots$,

$$n_{\mathrm{GGE}}(k_m) = \sum_{n=0}^{\infty} a_{n+m},$$

$$a_l = \exp\left\{-2\sum_{n=0}^{\infty}\frac{f(n)}{n}\right\}\sum_{m=0}^{\infty} c_m c_{m+l} = a_{-l},$$

$$c_m = \frac{1}{m}\sum_{l=1}^{m} f(l)c_{m-l},$$

$$f(l) = n_{\mathrm{B}}(\beta v_{\mathrm{F}}q_l) - 2c_{q_l}^2 s_{q_l}^2[n_{\mathrm{B}}(\beta v_{\mathrm{F}}q_l) - n_{\mathrm{B}}(\beta\omega_0)] \quad (42)$$

with $q_l=2\pi l/L$. As for the phonons we compare this result to the thermal distribution with temperature $\tilde{T}$. The canonical fermion distribution function of the interacting system can be computed along the same lines as the GGE distribution. Because of the involved structure, a comparison of the analytical expressions is less instructive as for the phonons. In Fig. 2 we therefore compare numerical results for the GGE with $\Gamma=0.01$, $\Omega=0.1$, system size parameter $\nu=2\pi/(Lq_{\mathrm{c}})=10^{-3}$, and dimensionless temperature $\tau=T/(v_{\mathrm{F}}q_{\mathrm{c}})=0.1$ with the best fit of a canonical distribution function for the same parameters—in particular, the *same* electron-phonon coupling and the *same* system size—and fitting parameter $\tilde{\tau}=\tilde{T}/(v_{\mathrm{F}}q_{\mathrm{c}})$. The best agreement is achieved for $\tilde{\tau}_{\mathrm{b}}=0.10275$. In general, $\tilde{\tau}_{\mathrm{b}}$ depends on the model parameters and τ. The differences are small but significant as becomes explicit in the inset which shows the absolute value of the difference of the two distributions. Doubling the system size does not lead to any changes on the scale of the main plot as well as the one of the inset. Thus the curves can be considered to be in the thermodynamic limit and the two ensembles

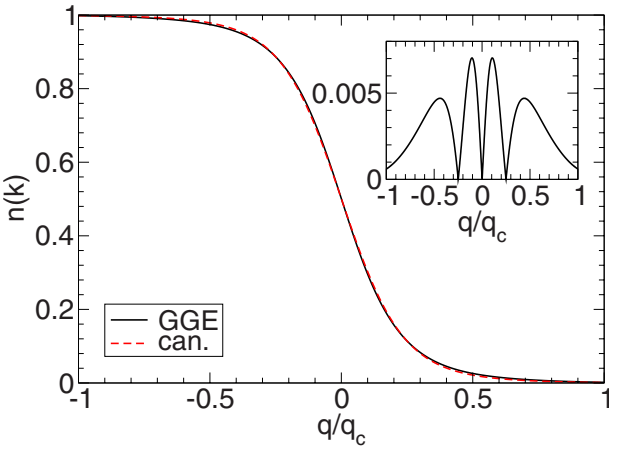

FIG. 2. (Color online) The GGE and canonical momentum distribution function of the fermions. The system parameters are $\Gamma=0.01$, $\Omega=0.1$, $\nu=2\pi/(Lq_{\mathrm{c}})=10^{-3}$ and the dimensionless initial temperature is $\tau=T/(v_{\mathrm{F}}q_{\mathrm{c}})=0.1$. The canonical distribution is the best fit to the GGE one with the fitted temperature $\tilde{\tau}_{\mathrm{b}}=0.10275$. The inset shows the absolute value of the difference of the two functions.

lead to different results even after the latter has been performed. This is a crucial observation as we have to distinguish this type of deviation between the predictions of two ensembles from the one which might appear at finite L but vanishes for $L\to\infty$. An example for the latter case is the difference between the canonical and the grand canonical ensembles as referred to in lectures on statistical mechanics. For noninteracting fermions with a linear dispersion such *finite-size* differences are explicitly studied in Ref. 38.

B. Expectation values for the k_0 excitation

We next derive the same expectation values but for the k_0 excitation. Using Eqs. (18), (19), (37), and (38) we obtain

$$\langle\hat{H}_{\mathrm{e}}\rangle_{\hat{\rho}_{\mathrm{GGE}}} = \sum_{q>0} v_{\mathrm{F}}q\frac{2\pi}{Lq}(c_q^4+s_q^4)\Theta(k_0-q),$$

$$\langle\hat{H}_{\mathrm{p}}\rangle_{\hat{\rho}_{\mathrm{GGE}}} = 2\omega_0\sum_{q>0}\frac{2\pi}{Lq}c_q^2 s_q^2\Theta(k_0-q),$$

$$\langle\hat{H}_{\mathrm{ep}}\rangle_{\hat{\rho}_{\mathrm{GGE}}} = 2g\sum_{q>0}\frac{2\pi}{Lq}\sqrt{q}c_q s_q(c_q^2-s_q^2)\Theta(k_0-q). \quad (43)$$

In contrast to the quench case, the energies are *not* extensive. This is related to the fact that even for $L\to\infty$ we only add a *single* additional fermion at momentum k_0 to the filled Fermi sea. The phonon momentum distribution function is given by

$$N_{\mathrm{GGE}}(q) = 2\frac{2\pi}{Lq}c_q^2 s_q^2\Theta(k_0-q). \quad (44)$$

Using the bosonization of the fermionic fields the GGE expectation value for the momentum distribution function follows as

$$n_{\mathrm{GGE}}(k) = \frac{1}{L}\int_{-L/2}^{L/2} dx e^{-ikx} \exp\left\{\sum_{q>0}\frac{2\pi}{Lq}e^{-iq(x-i0)}\right\} \times \exp\left\{2\sum_{q>0}\left(\frac{2\pi}{Lq}\right)^2 (c_q^4 + s_q^4) \times [1-\cos(qx)]\Theta(k_0-q)\right\}.$$

It is now crucial to realize that due to the factor $1/L^2$ in the exponent, the second term approaches 1 in the thermodynamic limit $L\to\infty$ independent of the electron-phonon coupling. In this limit, the remaining terms form a step function. We thus find

$$\lim_{L\to\infty} n_{\mathrm{GGE}}(k) = \Theta(k) \tag{45}$$

and the fermionic momentum distribution function of the GGE in the thermodynamic limit becomes equal to the one of the *ground state* (which for the present model is equal to the noninteracting one; see above). This is consistent with the observation that the energies for the k_0 excitation are not extensive. For finite L, $n_{\mathrm{GGE}}(k)$ can again be computed iteratively using Eq. (42) with $f(l)$ replaced by

$$f(l) = (c_{q_l}^4 + s_{q_l}^4)\Theta(k_0 - q_l)/l. \tag{46}$$

We note in passing that as for the quench for finite L, $n_{\mathrm{GGE}}(k)$ is *different* from the canonical distribution function obtained for the same system parameters at an optimally chosen temperature $\tilde{T}$. The same holds for $N_{\mathrm{GGE}}(q)$.

V. QUENCH DYNAMICS

We now investigate the dynamics of the density matrix and the expectation values considered above under the Hamiltonian Eq. (9) starting out from the *noninteracting* ($g=0$) canonical density matrix Eq. (26) at temperature $T=1/\beta$. Using the formal solution

$$\hat{\rho}^{\mathrm{q}}(t) = e^{-i\hat{H}t}\hat{\rho}_{\mathrm{i}}^{\mathrm{q}} e^{i\hat{H}t} \tag{47}$$

of the von Neumann equation and Eq. (19), we end up with

$$Z\hat{\rho}^{\mathrm{q}}(t) = \exp\left\{-\beta\sum_{q>0}\left[(v_{\mathrm{F}}qc_q^2 + \omega_0 s_q^2)\hat{\alpha}_q^\dagger\hat{\alpha}_q + c_q s_q(\omega_0 - v_{\mathrm{F}}q) \times e^{-i\Delta\lambda(q)t}\hat{\alpha}_q^\dagger\hat{\beta}_q + \mathrm{H.c.} + (v_{\mathrm{F}}qs_q^2 + \omega_0 c_q^2)\hat{\beta}_q^\dagger\beta_q\right]\right\}, \tag{48}$$

where

$$\Delta\lambda(q) = \lambda_+(q) - \lambda_-(q).$$

We emphasize that only the difference of the two eigenmode energies enters the dynamics. To compute the expectation values of interest with $\hat{\rho}^{\mathrm{q}}(t)$, one can now diagonalize the *time-dependent* 2×2 coefficient matrix of the quadratic form appearing in the exponent of Eq. (48) and introduce new *time-dependent* bosonic operators as linear combinations of the $\hat{\alpha}_q^{(\dagger)}$ and $\hat{\beta}_q^{(\dagger)}$. Alternatively, one can use Eqs. (23) and (24) and compute the expectation values with $\hat{\rho}_{\mathrm{i}}^{\mathrm{q}}$.

For the time dependence of the subsystem excess energies and interaction energy this leads to

$$\delta\langle\hat{H}_{\mathrm{e}}\rangle_{\hat{\rho}^{\mathrm{q}}(t)} = -\sum_{q>0} v_{\mathrm{F}}q 2c_q^2 s_q^2 \times [n_{\mathrm{B}}(\beta v_{\mathrm{F}}q) - n_{\mathrm{B}}(\beta\omega_0)][1-\cos\{\Delta\lambda(q)t\}],$$

$$\delta\langle\hat{H}_{\mathrm{p}}\rangle_{\hat{\rho}^{\mathrm{q}}(t)} = \omega_0\sum_{q>0} 2c_q^2 s_q^2 \times [n_{\mathrm{B}}(\beta v_{\mathrm{F}}q) - n_{\mathrm{B}}(\beta\omega_0)][1-\cos\{\Delta\lambda(q)t\}],$$

$$\langle\hat{H}_{\mathrm{ep}}\rangle_{\hat{\rho}^{\mathrm{q}}(t)} = 2g\sum_{q>0}\sqrt{q}c_q s_q(c_q^2 - s_q^2) \times [n_{\mathrm{B}}(\beta v_{\mathrm{F}}q) - n_{\mathrm{B}}(\beta\omega_0)][1-\cos\{\Delta\lambda(q)t\}]. \tag{49}$$

It is easy to show that for all t the total excess energy $\delta\langle\hat{H}\rangle_{\hat{\rho}^{\mathrm{q}}(t)}$ sums up to zero due to energy conservation. To answer the question if the (excess) energies become stationary in the long-time limit, we *first* perform the *thermodynamic limit*. Afterward the oscillatory terms average out for $t\to\infty$ when the momentum *integrals* are performed. For $L\to\infty$, the (excess) energy expectation values (per particle) thus become *stationary* and *equal* to the GGE expectation values (per particle) as determined in Eq. (39). This provides a first indication that for our model long-time expectation values of observables which become stationary can indeed be computed using the appropriate GGE. As discussed in Sec. I in performing the thermodynamic limit one often keeps the size of one of the subsystems (the $\mathcal{S}$) containing the relevant local observables fixed while the thermodynamic limit is performed in its complement, the environment $\mathcal{E}$.[9] In our model, the limit $L\to\infty$ is simultaneously performed in the fermion and phonon subsystems (quantization of momenta).

As shown in Fig. 3 (solid lines) for large t, the energies oscillate around their asymptotic GGE values (dashed lines) with seemingly a single frequency and a slowly decaying amplitude. From the data it is obvious that a rather good approximation for the stationary expectation values can be obtained by averaging the (excess) energies over a time interval which is much larger than the inverse oscillation frequency and starts at a sufficiently large time.

Analytic insights on the long-time behavior can be gained by applying the techniques of *asymptotic analysis*[39] such as the *stationary phase method* to the momentum integrals in Eq. (49). Using the latter, one can show that for not too strong couplings $2\Gamma<\Omega$ (on which we mainly focus) such that the stationary point of $\Delta\lambda(q)$ lies inside the integration interval $(0,q_c)$ the dominant oscillation frequency (at large times) is given by the *minimum* of the mode energy difference,

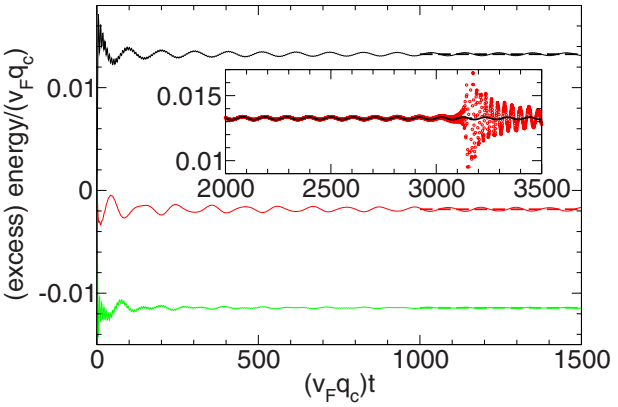

FIG. 3. (Color online) Time evolution of the (excess) energies in the fermion (solid line, top) and phonon (solid line, middle) subsystems as well as of the energy in the interacting part of the Hamiltonian (solid line, bottom). The dashed lines for $t \in [1000, 1500]$ are the corresponding GGE expectation values. The parameters are $\Gamma=0.01$, $\Omega=0.1$ and the initial temperature is given by $\tau=0.1$. The symbols in the inset show data for the energy in the fermion subsystem obtained at a finite system size $\nu=2\times10^{-3}$. The recurrence time is then given by $(v_F q_c)t_r=v_F 2\pi/(L\nu)L/v_F=2\pi/\nu\approx3142$.

$$\frac{\Delta\lambda(q_{\min})}{v_F q_c} = 2\Gamma\sqrt{\frac{\Omega}{\Gamma}-1}$$

and the amplitude falls off as $1/\sqrt{t}$.[21] The convergence toward the stationary values is thus rather slow. Furthermore, the second (high) frequency visible at small times results from a contribution of the boundaries of the momentum integrals and can be identified as $\Delta\lambda(q_c)$. The mode energy difference of the lower boundary does not appear as a frequency as the corresponding amplitude vanishes.

For comparison the inset of Fig. 3 also contains results for the energy in the electron subsystem obtained at *finite* L (symbols). Obviously on the scale $t_r=L/v_F$ finite size effects set in and the oscillations become rather erratic. Remarkably, for upper times not too large compared to t_r the $L\to\infty$ asymptotic value can still be extracted accurately by averaging over the time even beyond t_r. The same holds for the other energy expectation values.

From the energy in the phonon subsystem Eq. (49), the time evolution of the phonon momentum distribution function out of the initial Bose function $n_B(\beta\omega_0)$ can be read off

$$\delta N_q(q,t) = N_q(q,t) - n_B(\beta\omega_0) = 2c_q^2 s_q^2 [n_B(\beta v_F q) - n_B(\beta\omega_0)][1-\cos\{\Delta\lambda(q)t\}]. \tag{50}$$

As the phononic annihilation and creation operators are *linear* combinations of the eigenmode ladder operators [see Eq. (19)] it is not surprising, that the phonon momentum distribution function for a fixed q does not become stationary; it shows a sinusoidal oscillation with frequency $\Delta\lambda(q)$ and fixed amplitude for all t. The time-dependent part $\delta N_q(q,t)$ is shown in Fig. 4 for $\Gamma=0.01$, $\Omega=0.2$, and temperature $\tau=0.1$. The shape for fixed t can be understood from Fig. 1 (in which s_q^2 and c_q^2 are shown) and the q dependence of the

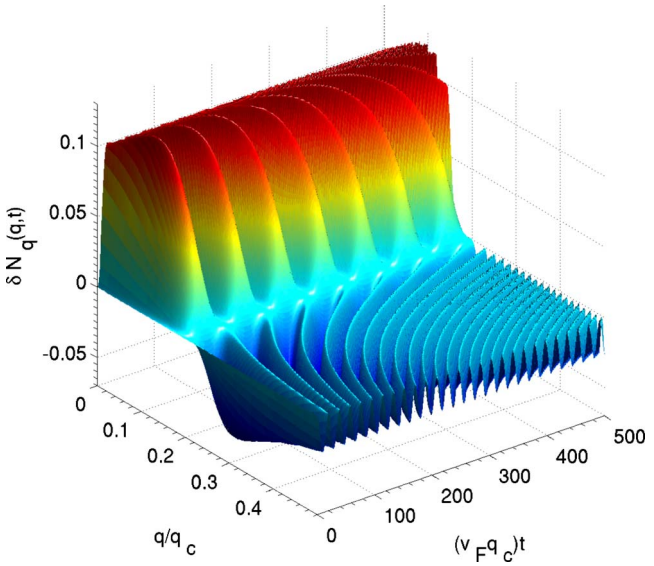

FIG. 4. (Color online) The time-dependent part of the phonon momentum distribution function $\delta N_q(q,t)$ as a function of q and t. The parameters are $\Gamma=0.01$, $\Omega=0.2$, and the initial temperature is given by $\tau=0.1$.

difference of the two Bose functions. Only after averaging over a small interval Δq around q, $N_q(q,t)$ becomes stationary at large times as the cosine term drops out.

This behavior has to be contrasted to the one of the fermion momentum distribution function $n_q(k,t)$. By the bosonization of the field operator (see Sec. III) the relation between the $\hat{a}_k^{(\dagger)}$ and the eigenmode ladder operators is highly nonlinear and it is not clear *a priori* whether or not $n_q(k,t)$ becomes stationary. Using the methods introduced above we obtain

$$n_q(k,t) = \frac{1}{L}\int_{-L/2}^{L/2} dx e^{-ikx} \exp\left\{\sum_{q>0}\frac{2\pi}{Lq}e^{-iq(x-i0)}\right\} \times\exp\left\{-\sum_{q>0}\frac{4\pi}{Lq}[1-\cos(qx)]n_B(\beta v_F q)\right\} \times\exp\left\{\sum_{q>0}\frac{8\pi}{Lq}c_q^2 s_q^2[1-\cos(qx)] \times[n_B(\beta v_F q)-n_B(\beta\omega_0)][1-\cos\{\Delta\lambda(q)t\}]\right\}. \tag{51}$$

First taking the thermodynamic limit and subsequently the long-time limit, the oscillatory time-dependent term again averages out and we find *convergence* to the GGE expectation value Eq. (41),

$$\lim_{t\to\infty}\lim_{L\to\infty} n_q(k,t) = \lim_{L\to\infty} n_{GGE}(k).$$

Furthermore, an analytic stationary phase analysis similar to the one performed for the energies shows that for sufficiently large t and fixed k, $n_q(k,t)$ oscillates with frequency $\Delta\lambda(q_{\min})$ around $n_{GGE}(k)$ with an amplitude which decays as $1/\sqrt{t}$. As

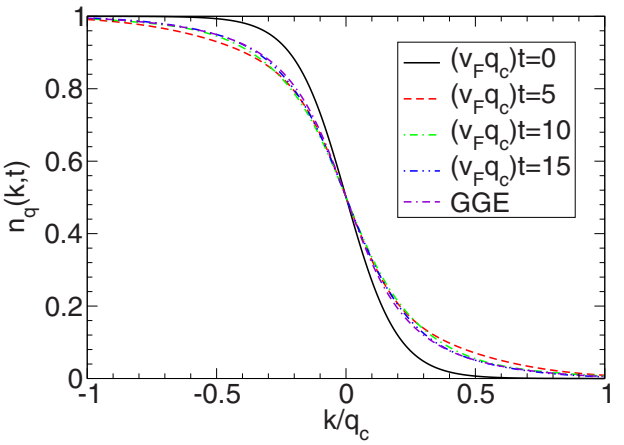

FIG. 5. (Color online) Momentum distribution function of the fermions as a function of k for different t. The GGE distribution obtained for the same system size is shown for comparison. The parameters are $\Gamma=0.03$, $\Omega=0.1$, $\nu=10^{-3}$, and the initial temperature is given by $\tau=0.1$.

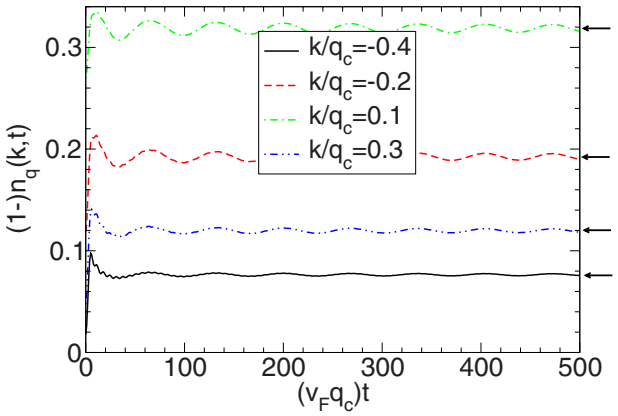

FIG. 6. (Color online) The same as in Fig. 5 but as a function of t for different k. For the momenta $k<0$, $1-n_q(k,t)$ is shown. The GGE expectation values are indicated by the arrows.

for the energies the second relevant frequency is $\Delta\lambda(q_c)$.

For finite (but large) L, $n_q(k,t)$ can again efficiently be computed numerically using the recursion relation Eq. (42) with $f(l)$ replaced by

$$f(l) = n_B(\beta v_F q_l) - 2c_{q_l}^2 s_{q_l}^2 [n_B(\beta v_F q_l) - n_B(\beta\omega_0)] \times [1 - \cos\{\Delta\lambda(q_l)t\}]. \quad (52)$$

In Fig. 5, the time evolution of the fermion momentum distribution function as a function of k and a few t is compared to the GGE prediction obtained for the same system length L. In Fig. 6, we show $n_q(k,t)$ for a few fixed k as a function of t. Almost independent of the system parameters, the temperature, and the considered momentum the asymptotic behavior analytically described above (for $L\to\infty$) sets in very quickly and holds for times $t<t_r$ (oscillation frequencies and $1/\sqrt{t}$ decay). Just as for the energies the asymptotic values of $n_q(k,t)$ for large t and fixed k can be determined very accurately by averaging over an appropriate time interval. Similar to the behavior found for the energies, the oscillations of $n_q(k,t)$ for fixed k become rather erratic if one exceeds t_r (not shown here) but time averaging still gives very good agreement with the GGE result. Doubling the system size for the results shown in Figs. 5 and 6 does not lead to any changes on the scale of the plots and the curves can considered to be in the thermodynamic limit [as long as $t<t_r$ which is clearly the case in the figures; $(v_F q_c)t_r \approx 6284$].

We can conclude that for the quench and the observables of interest in the present work, which relax to a stationary value, the latter is equal to the GGE prediction. The GGE expectation value differs from a thermal one (see the discussion in Sec. IV, in particular, Fig. 2). In the long-time limit, the expectation values of the (subsystem) energies and the momentum distribution function of the fermions at every (fixed) k oscillate around the GGE result with a frequency $\Delta\lambda(q_{min})$ and an amplitude decaying as $1/\sqrt{t}$. In this respect, the dynamics is rather simple—in particular, compared to the one resulting from the k_0 excitation discussed in the next section.

We briefly comment on the relation of our calculations to those performed in the bosonization approach to the purely electronic Tomonaga-Luttinger model (in and out of equilibrium). For this model q sums (integrals) of the type appearing in Eq. (51) are usually performed analytically after *Taylor expanding* the renormalized bosonic dispersion [here $\Delta\lambda(q)$] to *linear order* in q and *assuming* a particular q dependence of the s_q^2. It is generally believed that these steps do not alter the low-energy physics of the model. However, in Ref. 40 it was shown that this is not correct and the typical Tomonaga-Luttinger liquid exponents are affected by these approximations. In particular, this implies that the validity of the very interesting study of the relaxation dynamics of Ref. 5 is more restricted than it is realized by the author(s). For the present model it is obvious that similar approximations would strongly alter the physics as the nonlinearity of $\Delta\lambda(q)$ lies at the heart of our results.

VI. DYNAMICS OF THE k_0 EXCITATION

Using the methods introduced above for the k_0 excitation, the expectation values of the observables studied here have been computed in Ref. 25. We emphasize that in this paper only the short-time behavior was investigated while we are (mainly) interested in the long-time asymptotics. For completeness we here present the relevant expressions taken from Ref. 25.

The time dependence of the (subsystem) energies is given by

$$\langle \hat{H}_e \rangle_{\hat{\rho}^{k_0(t)}} = \sum_{q>0} v_F q \frac{2\pi}{Lq} [c_q^4 + s_q^4 + 2c_q^2 s_q^2 \times \cos\{\Delta\lambda(q)t\}]\Theta(k_0 - q),$$

$$\langle \hat{H}_p \rangle_{\hat{\rho}^{k_0(t)}} = 2\omega_0 \sum_{q>0} \frac{2\pi}{Lq} c_q^2 s_q^2 [1 - \cos\{\Delta\lambda(q)t\}]\Theta(k_0 - q),$$

$$\langle \hat{H}_{\rm ep}\rangle_{\hat{\rho}^{k_0(t)}} = 2g\sum_{q>0}\frac{2\pi}{Lq}\sqrt{q}c_q s_q(c_q^2 - s_q^2) \times[1-\cos\{\Delta\lambda(q)t\}]\Theta(k_0-q). \quad (53)$$

After the thermodynamic limit has been performed in the long-time limit, the energy expectation values approach the GGE ones Eq. (43) in an oscillatory fashion with the dominant frequency $\Delta\lambda(q_{\rm min})$ and an amplitude decaying as $1/\sqrt{t}$. This can be shown analytically applying the same methods as used for the quench. A typical example for the time evolution of the energies is given in Fig. 1 of Ref. 25.

For the phonon dynamics, one obtains

$$N_{k_0}(q,t) = 2\frac{2\pi}{Lq}c_q^2 s_q^2[1-\cos\{\Delta\lambda(q)t\}]\Theta(k_0-q). \quad (54)$$

For the reason discussed in the last section, the phonon momentum distribution function does not become stationary. A plot of $N_{k_0}(q,t)$ similar to our Fig. 4 (obtained for the quench) is shown in Fig. 2 of Ref. 25.

To compute $n_{k_0}(k,t)$ for the initial state containing a highly excited fermion in addition to the filled Fermi sea, one has to bosonize *four* fermion fields instead of two. This leads to a rather involved expression for the fermion momentum distribution function as discussed in detail in the Appendix of Ref. 25. In contrast to the quench this expression does not provide much analytical insight and, in particular, does not allow to analytically conclude, that in the long-time limit $n_{k_0}(k,t)$ becomes equal to the GGE expectation value (at least after taking $L\to\infty$ first). We thus have to rely on numerical comparisons. Therefore, here we only give the equations needed for an iterative numerical calculation of $n_{k_0}(k,t)$ for finite L,[25]

$$n_{k_0}(k_n,t) = \sum_{r=\max(n,0)}^{n_0}\sum_{s=0}^{n_0-r}\sum_{l=0}^{\min(r+s,r-n)} a_{r+s-l}^{(n_c)}(t) \times[a_r^{(n_c)}(t)]^* b_l^{(n_c)}(t)[b_s^{(n_c)}(t)]^*, \quad (55)$$

for $n_0 \geq n > 0$ and $n_c = \frac{q_c L}{2\pi}$. The time-dependent coefficients $a_n^{(m)}$ and $b_n^{(m)}$ are determined for $m>1$, $l\in\mathbb{N}_0$, and $i=0,\ldots,m-1$ by

$$a_{lm+i}^{(m)}(t) = \sum_{j=0}^{l}\frac{[u_m(t)/m]^j}{j!}a_{m(l-j)+i}^{(m-1)}(t),$$

$$b_{lm+i}^{(m)}(t) = \sum_{j=0}^{l}\frac{[-u_m(t)/m]^j}{j!}b_{m(l-j)+i}^{(m-1)}(t) \quad (56)$$

with the starting values $(m=1)$

$$a_l^{(1)}(t) = \sum_{k=0}^{l}[e(t)]^{l-k}\frac{[u_1(t)]^k}{k!}, \quad l\in\mathbb{N}_0,$$

$$b_l^{(1)}(t) = \frac{[-u_1(t)]^l}{l!} - \frac{[-u_1(t)]^{l-1}}{(l-1)!}e(t), \quad l\in\mathbb{N},$$

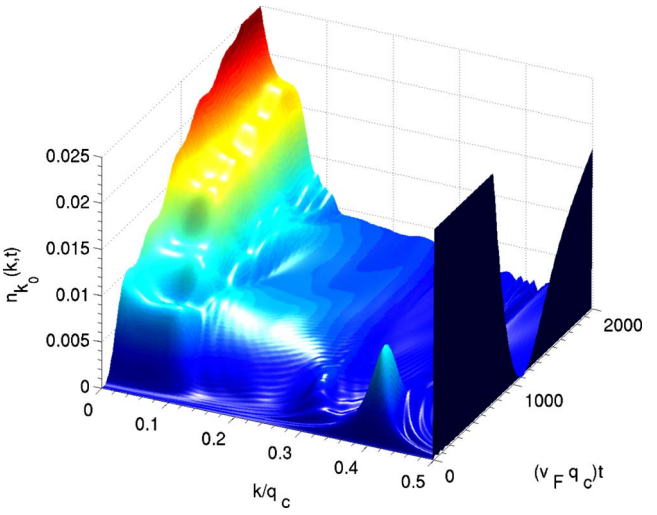

FIG. 7. (Color online) The momentum distribution function of the fermions $n_{k_0}(k,t)$. The parameters are $\Gamma=0.001$, $\Omega=0.1$, $\nu=10^{-3}$, and $k_0/q_c=0.5$. The dark feature at $k=k_0$ is the occupation of the initially filled level which strongly exceeds the scale of the z axis. Note the scale of the z axis.

$$b_0^{(1)}(t) = 1. \quad (57)$$

The functions $u_l(t)$ and $e(t)$ are defined as

$$u_l(t) = c_{q_l}^2 e^{-i\lambda_+(q_l)t} + s_{q_l}^2 e^{-i\lambda_-(q_l)t} - e^{-iv_F q_l t},$$

$$e(t) = e^{-iv_F t 2\pi/L}. \quad (58)$$

In contrast to all our earlier expressions for the time dependence of expectation values, both eigenenergies $\lambda_\pm(q)$ enter explicitly and not only their difference $\Delta\lambda(q)$. This leads to very rich dynamics.

Figures 7 and 8 show two examples of $n_{k_0}(k,t)$ for a weak $(\Gamma=0.001)$ and an intermediate $(\Gamma=0.01)$ electron-phonon coupling at finite but large L. Only the part $0\leq k\leq k_0$ is shown; for the time evolution of initially filled momenta see

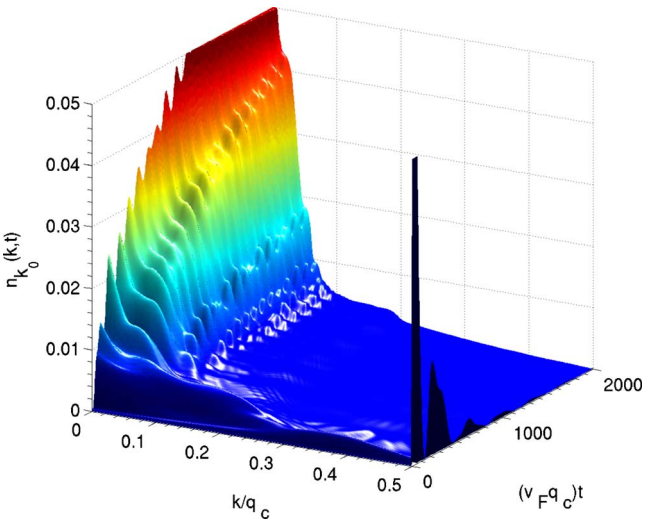

FIG. 8. (Color online) The same as in Fig. 7 but for $\Gamma=0.01$.

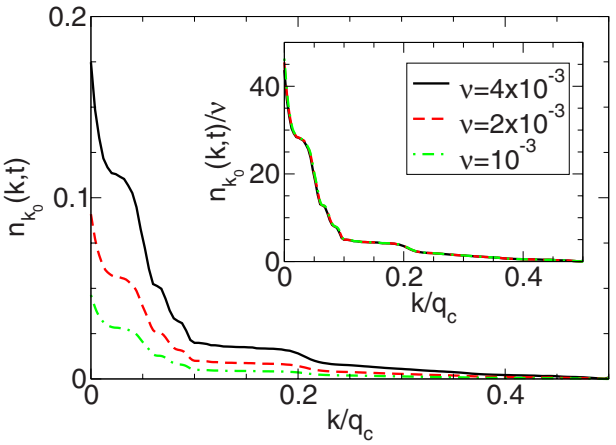

FIG. 9. (Color online) The momentum distribution function of the fermions $n_{k_0}(k,t)$ as a function of $k>0$ for fixed $(v_F q_c)t=10^3$ and different $\nu=4\times10^{-3}$, 2×10^{-3}, 10^{-3}. The other parameters are $\Gamma=0.01$, $\Omega=0.1$, and $k_0/q_c=0.5$. The inset shows $n_{k_0}(k,t)/\nu$.

Figs. 10 and 11. At $t=0$ only, the momenta $k<0$ and k_0 are occupied (with weight 1) and no phonons are present. The hot electron decays into states with lower energy by producing phonons. The energy conservation in individual scattering processes is not sharp on short time scales which leads to *broadened replicas* of the initial k_0 excitation at momenta k_0-nq_B, with $n\in\mathbb{N}$ and $q_B=\omega_0/v_F$. This is reminiscent to the derivation of Fermi's golden rule. In time-dependent perturbation theory, the transition probability between two energy eigenstates with energy difference $\Delta\omega$ is proportional to $[\sin(\Delta\omega t/2)/(\Delta\omega/2)]^2$ which only at large t becomes an energy conserving δ function. Thus the replicas sharpen for larger times. For our model, they never reach the width of the original excitation before they get depleted again. Details of this dynamics are discussed in Ref. 25. Two of such replica are visible in Fig. 7 for small g while only a very broad feature appears for intermediate couplings (see Fig. 8). As soon as phonons are generated they couple to fermions in the

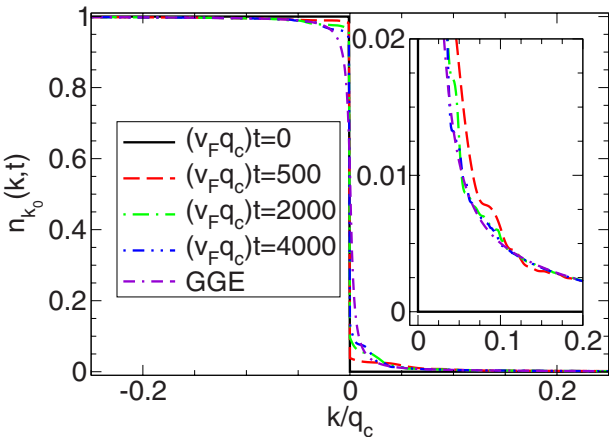

FIG. 10. (Color online) Momentum distribution function of the fermions $n_{k_0}(k,t)$ as a function of k for different t. The GGE distribution obtained for the same system size is shown for comparison. The parameters are $\Gamma=0.03$, $\Omega=0.1$, $\nu=10^{-3}$, and $k_0/q_c=0.5$.

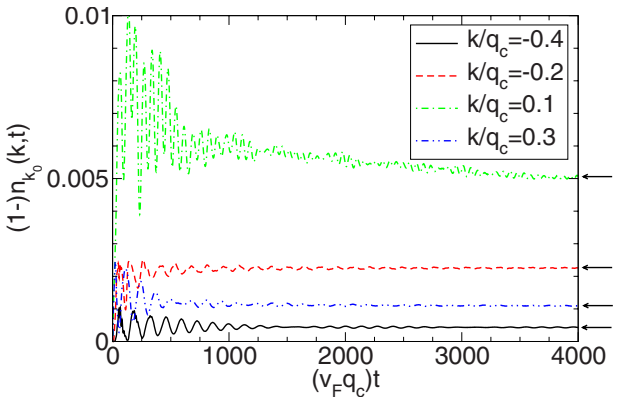

FIG. 11. (Color online) The same as in Fig. 10 but as a function of t for different k. For the momenta $k<0$, $1-n_{k_0}(k,t)$ is shown. The GGE expectation values are indicated by the arrows.

filled Fermi sea (at $k<0$; not shown in the figures) and excite them to higher energies. This leads to a steplike feature of width q_B at small $k>0$ and $t>0$. For increasing time, the sharp initial jump at $k=0$ from 1 to 0 is smoothened. In particular, the occupancies of the levels at $k\gtrapprox0$ which are 0 at $t=0$ will increase significantly. In Figs. 7 and 8 this is reflected in the continuing overall increase in $n_{k_0}(k,t)$ for small fixed k on time scales $[(v_F q_c)t\approx10^3]$ at which saturation is already clearly established for the quench dynamics (see Figs. 5 and 6). The initially filled level at k_0 is depleted but subsequently refilled on a time scale which obviously depends on the electron-phonon coupling (compare Figs. 7 and 8). For large times $n_{k_0}(k_0,t)$ approaches a small value in an oscillatory fashion. For the quench the frequency with which $n_q(k,t)$ oscillates (at fixed k) is independent of k and given by $\Delta\lambda(q_{\min})$. In contrast from Figs. 7 and 8 it is obvious that for the present initial nonequilibrium state (and on the same time scales as for the quench) different frequencies appear (compare the behavior at small k and k close to k_0; see also Fig. 11). We conclude that the dynamics generated by the k_0 excitation is significantly richer then the one found after a quench.

Before comparing numerical data for $n_{k_0}(k,t)$ to the GGE result $n_{\mathrm{GGE}}(k)$, we have to gain a detailed understanding of the subtleties of the thermodynamic limit for the present nonequilibrium initial state. We already noted that regardless of the electron-phonon coupling in the thermodynamic limit $n_{\mathrm{GGE}}(k)$ is given by the ground-state expectation value; the noninteracting step function. This result is consistent with our finding that the excess energies (both the GGE ones and the time-evolved ones) are not extensive. We only add the L-independent energy $v_F k_0$ to the energy of the filled Fermi sea (the ground state). As the energy is conserved, the three terms Eq. (53) add up to $v_F k_0$ for all $t\geq0$. Based on these considerations and our previous results, we expect that

$$\lim_{t\to\infty}\lim_{L\to\infty} n_{k_0}(k,t)=\Theta(k)$$

in accordance with the GGE prediction. This is confirmed by Fig. 9 which shows $n_{k_0}(k,t)$ as a function of $k\geq0$ for fixed $(v_F q_c)t=10^3$ and different $\nu=4\times10^{-3}$, 2×10^{-3}, 10^{-3}. In the

inset, we plot $n_{k_0}(k,t)/\nu$ and the collapse of the three curves indicates that $n_{k_0}(k,t)$ for $k>0$ vanishes as $1/L$. The same holds for $1-n_{k_0}(k,t)$ at $k<0$.

After clarifying the behavior in the thermodynamic limit, we now compare the time-evolved and GGE distribution functions for fixed $L<\infty$. In Fig. 10, we show the momentum distribution function as a function of k for a few fixed t, the same model parameters as in Fig. 5 (quench), and $k_0/q_c=0.5$. Up to very small momenta $|k|\ll q_c$ (see the inset), we find convergence toward the GGE prediction for times $t<t_r$. As argued above the changes during the time evolution for the small momenta are large (from a step function at $t=0$ to a continuous function at large t) and convergence cannot be found for times $t<t_r$. Note that because of the slow convergence the times shown in Fig. 10 are much larger than those of Fig. 5 even though the model parameters are the same in both figures. Finally, in Fig. 11 we show $n_{k_0}(k,t)$ for a few fixed k as a function of t. The GGE expectation values are indicated by the arrows. For k sufficiently far away from the initial step at $k=0$, it is again evident that $n_{k_0}(k,t)$ approaches $n_{\mathrm{GGE}}(k)$. In that sense a quasistationary state (finite L) is reached with a time averaged expectation value (over "large" times smaller than t_r) which can accurately be described by the GGE prediction and which is different from the step function reached in the thermodynamic limit. In complete analogy to our earlier findings for the quench dynamics extending the time beyond t_r leads to enhanced oscillations with a time average which is still close to $n_{\mathrm{GGE}}(k)$.

We note in passing that for the strongest possible electron-phonon coupling allowed by stability $\Gamma=\Omega$, $\lambda_-(q)=0$ for all $q<q_c$. A similar situation is discussed in Ref. 9. In this case, the amplitude of the oscillation in $n_{k_0}(k,t)$ for fixed k does *not* decay. The energies still approach a constant large time limit but with a $1/t$ instead of a $1/\sqrt{t}$ decay.[41]

We did not succeed in extracting analytical results for the long-time asymptotics from the rather involved finite-L expression for $n_{k_0}(k,t)$ presented in the Appendix of Ref. 25. A numerical analysis for curves which at sufficiently large times (but still $t<t_r$) oscillate around the finite L GGE prediction (e.g., the $k/q_c=-0.4$, -0.2, and 0.3 curves in Fig. 11) shows that the amplitude decays *faster* than in the case of a quench, that is faster than $1/\sqrt{t}$. This has to be contrasted to the observation that it takes much *longer* times in case of the k_0 excitation before any asymptotic behavior sets in (compare Figs. 6 and 11). From the numerical data it turned out to be impossible to extract an analytical form of the amplitude decay (e.g., power law $1/t^{\chi}$ with an exponent χ larger than 1/2). As already noted when discussing Figs. 7 and 8, the oscillation frequency of $n_{k_0}(k,t)$ at fixed k seems to dependent on k. This becomes even more evident in Fig. 11. Besides this the oscillation frequency depends on the model parameters Γ and Ω. We did not succeed in extracting a clear picture for the dependence of the frequencies on these three parameters. In addition, it is not obvious how to relate the numerically determined frequencies appearing in $n_{k_0}(k,t)$ at fixed k to the mode energies $\lambda_+(q)$ and $\lambda_-(q)$. This again exemplifies that the time evolution of the fermionic momentum distribution function for the k_0 excitation is rather involved and much richer than the dynamics encountered above.

VII. SUMMARY

We studied the relaxation dynamics of an exactly solvable electron-phonon model out of two initial nonequilibrium states. This way we added a *continuum* model containing both *fermions and bosons* to the list of quantum many-body models recently investigated and considered other nonequilibrium situations than the parameter quench. Our model features a natural set of constants of motion, with as many elements as degrees of freedom. This set can be used to construct the initial-state-dependent generalized Gibbs ensemble. We found that for *all observables* of interest to us the asymptotic long-time limit of expectation values which *become stationary* are equal to those obtained from the appropriate *natural GGE*. We discussed that the momentum distribution functions of the GGE differ from those obtained within the canonical ensemble. While the (excess) energies and the electron momentum distribution function become stationary, the phonon momentum distribution at fixed momentum oscillates with a constant amplitude even at large times. This can be understood from the linear relation between the eigenmode ladder operators and the phononic ones. Long-time convergence of the energies and the fermionic momentum distribution function in the strict sense is only achieved if the thermodynamic limit is taken first. Going beyond this we showed that the GGE predictions for these expectation values agree to time-averaged values taken at large times (even larger than the characteristic scale $t_r=L/v_F$). For most of the studied situations, we were able to *analytically* describe how the GGE prediction is reached. We found that the asymptotic limit is only reached following a power law (instead of exponentially). The dynamics of the fermionic momentum distribution function resulting from the k_0 excitation turned out to be much richer than the one found for other observables and for the interaction quench.

ACKNOWLEDGMENTS

We are grateful to D. Schuricht, S. Manmana, M. Kollar, F. Göhmann, and A. Muramatsu for very useful discussions and to D. Schuricht for reading the manuscript prior to submission. Technical support by S. Grap and C. Karrasch is acknowledged. We thank K. Schönhammer for an earlier collaboration with one of us (V.M.) which is of fundamental importance for the present work. We thank the Deutsche Forschungsgemeinschaft (Forschergruppe 912) for support.

[1] E. T. Jaynes, Phys. Rev. **106**, 620 (1957).
[2] M. Greiner, O. Mandel, T. W. Hänsch, and I. Bloch, Nature (London) **419**, 51 (2002); T. Kinoshita, T. Wenger, and D. S. Weiss, *ibid.* **440**, 900 (2006); L. E. Sadler, J. M. Higbie, S. R. Leslie, M. Vengalattore, and D. M. Stamper-Kurn, *ibid.* **443**, 312 (2006).
[3] M. Rigol, A. Muramatsu, and M. Olshanii, Phys. Rev. A **74**, 053616 (2006).
[4] M. Rigol, V. Dunjko, V. Yurovsky, and M. Olshanii, Phys. Rev. Lett. **98**, 050405 (2007).
[5] M. A. Cazalilla, Phys. Rev. Lett. **97**, 156403 (2006); A. Iucci and M. A. Cazalilla, Phys. Rev. A **80**, 063619 (2009).
[6] E. Perfetto, Phys. Rev. B **74**, 205123 (2006).
[7] M. Cramer, C. M. Dawson, J. Eisert, and T. J. Osborne, Phys. Rev. Lett. **100**, 030602 (2008).
[8] D. M. Gangardt and M. Pustilnik, Phys. Rev. A **77**, 041604(R) (2008).
[9] T. Barthel and U. Schollwöck, Phys. Rev. Lett. **100**, 100601 (2008).
[10] M. Eckstein and M. Kollar, Phys. Rev. Lett. **100**, 120404 (2008).
[11] M. Kollar and M. Eckstein, Phys. Rev. A **78**, 013626 (2008).
[12] C. Kollath, A. M. Läuchli, and E. Altman, Phys. Rev. Lett. **98**, 180601 (2007).
[13] S. R. Manmana, S. Wessel, R. M. Noack, and A. Muramatsu, Phys. Rev. Lett. **98**, 210405 (2007).
[14] M. Cramer, A. Flesch, I. P. McCulloch, U. Schollwöck, and J. Eisert, Phys. Rev. Lett. **101**, 063001 (2008).
[15] A. Flesch, M. Cramer, I. P. McCulloch, U. Schollwöck, and J. Eisert, Phys. Rev. A **78**, 033608 (2008).
[16] P. Barmettler, M. Punk, V. Gritsev, E. Demler, and E. Altman, Phys. Rev. Lett. **102**, 130603 (2009).
[17] M. Rigol, Phys. Rev. Lett. **103**, 100403 (2009).
[18] M. Moeckel and S. Kehrein, Phys. Rev. Lett. **100**, 175702 (2008).
[19] A. Hackl and S. Kehrein, J. Phys.: Condens. Matter **21**, 015601 (2009).
[20] P. Calabrese and J. Cardy, J. Stat. Mech.: Theory Exp. 2007, P06008.
[21] D. Fioretto and G. Mussardo, arXiv:0911.3345 (unpublished).
[22] J. Lancaster and A. Mitra, Phys. Rev. E **81**, 061134 (2010).
[23] F. Rossi and T. Kuhn, Rev. Mod. Phys. **74**, 895 (2002).
[24] C. Fürst, A. Leitenstorfer, A. Laubereau, and R. Zimmermann, Phys. Rev. Lett. **78**, 3733 (1997).
[25] V. Meden, C. Wöhler, J. Fricke, and K. Schönhammer, Phys. Rev. B **52**, 5624 (1995).
[26] V. Meden, J. Fricke, C. Wöhler, and K. Schönhammer, Z. Phys. B: Condens. Matter **99**, 357 (1996).
[27] D. Loss and D. P. DiVincenzo, Phys. Rev. A **57**, 120 (1998).
[28] S. Tomonaga, Prog. Theor. Phys. **5**, 544 (1950); J. M. Luttinger, J. Math. Phys. **4**, 1154 (1963); D. C. Mattis and E. H. Lieb, J. Math. Phys. **6**, 304 (1965).
[29] F. D. M. Haldane, J. Phys. C **14**, 2585 (1981).
[30] J. Sólyom, Adv. Phys. **28**, 201 (1979).
[31] G. Wentzel, Phys. Rev. **83**, 168 (1951).
[32] S. Engelsberg and B. B. Varga, Phys. Rev. **136**, A1582 (1964).
[33] M. Apostol and I. Baldea, J. Phys. C **15**, 3319 (1982); Phys. Lett. A **88**, 73 (1982).
[34] V. Meden, K. Schönhammer, and O. Gunnarsson, Phys. Rev. B **50**, 11179 (1994).
[35] V. Meden, Ph.D. thesis, Universität Göttingen, 1996.
[36] R. de L. Kronig, Physica (Amsterdam) **2**, 968 (1935).
[37] N. D. Mermin, J. Math. Phys. **7**, 1038 (1966).
[38] K. Schönhammer and V. Meden, Am. J. Phys. **64**, 1168 (1996).
[39] S. A. Orszag and C. M. Bender, *Advanced Mathematical Methods for Scientists and Engineers* (Springer, New York, 1999).
[40] V. Meden, Phys. Rev. B **60**, 4571 (1999).
[41] D. M. Kennes, Bachelor thesis, RWTH Aachen University, 2009.